ACS APPLIED MATERIALS & INTERFACES

Research Article

www.acsami.org

2,6-Bis(1-methylbenzimidazol-2-yl)pyridine: A New Ancillary Ligand for Efficient Thiocyanate-Free Ruthenium Sensitizer in Dye-Sensitized Solar Cell Applications

Surya Prakash Singh,*[,†] K. S. V. Gupta,[†] M. Chandrasekharam,[†] Ashraful Islam,[‡] Liyuan Han,[‡] Shinpei Yoshikawa,[§] Masa-aki Haga,[§] M. S. Roy,[▽] and G. D. Sharma*[,⊥]

[†]Inorganic & Physical Chemistry Division, CSIR-Indian Institute of Chemical Technology, Uppal Road, Tarnaka 500607, Hyderabad, India

[‡]Photovoltaic Materials Unit, National Institute for Materials Science, 1-2-1 Sengen, Tsukuba, Ibaraki 305-0047, Japan

[§]Department of Applied Chemistry, Faculty of Science and Engineering, Chuo University, 1-13-27 Kasuga, Bunkyo-ku 112-8551, Tokyo, Japan

[▽]Defence Laboratory, Jodhpur 342011, Rajasthan, India

[⊥]R&D Center for Engineering and Science, JEC Group of Colleges, Jaipur Engineering College, Kukas, Jaipur 303101, Rajasthan, India

ABSTRACT: We have designed and synthesized a new thiocyante-free ruthenium complex containing 2,6-bis(1-methylbenzimidazol-2-yl)pyridine, coded as **SPS-G3**, and it has been used as an efficient photosensitizer for dye-sensitized solar cells (DSSCs). Upon sensitization of **SPS-G3** on nanocrystalline TiO_2 film, the DSSC test cell yielded a large short-circuit photocurrent (16.15 mA cm^{-2}), an open circuit voltage of 0.52 V, and a fill factor (FF) of 0.72, resulting in an overall power conversion efficiency (PCE) of 6.04% under simulated AM 1.5 solar irradiation (100 mW cm^{-2}). DSSCs were prepared by adding various concentrations of multiwall carbon nanotubes (MWCNTs) (up to 0.5 wt %) into the TiO_2 nanoparticles. Optimization of MWCNT concentration (0.3 wt %) lead to PCE values as high as 7.76%, while the test cells employing pure TiO_2 photoanode obtained an efficiency of 6.04%. The results indicate that the PCE of MWCNTs/TiO_2 composite DSSCs are dependent on the quantity of MWCNTs loading on the photoanodes. A small amount (0.3 wt %) clearly enhances the PCE of DSSC, while the excessive MWCNT loading lowers the photovoltaic performance of the DSSC. The increase in the PCE has been attributed to the decrease in charge-transport resistance, charge-transport time, and electron lifetime, which are estimated from electrochemical impedance spectra.

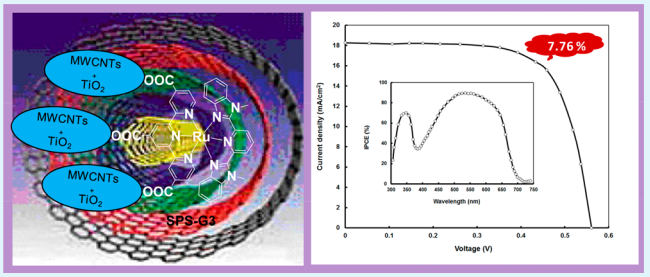

KEYWORDS: *dye-sensitized solar cells, ruthenium dye, MWCNTs, TiO_2, power conversion efficiency, thiocyante-free*

INTRODUCTION

Dye-sensitized solar cells (DSSCs) based on nanocrystalline TiO_2 have attracted increasing interest, because of their low cost of manufacturing and high power conversion efficiency (PCE), and they are considered to be promising candidates for next-generation solar cells.[1] A typical DSSC consist of a photoanode prepared from mesoporous TiO_2 particle adsorbed with a sensitizer, iodide/tri-iodide (I^-/I_3^-) redox couple as an electrolyte, and a platinum (Pt) counter electrode. Sensitizers play a critical role in the photovoltaic performance of DSSCs, which are required to have anchoring group for efficient electronic communication with TiO_2. Suitable matching of the highest occupied molecular orbital (HOMO) and lowest unoccupied molecular orbital (LUMO) energy levels of the sensitizer with the conduction band edge of TiO_2 and redox potential of electrolyte, broad absorption of sensitizer in solar spectra, and high molecular extinction coefficient are also essential.[2−8] Less-expensive metal-free organic dyes have achieved significant progress in recent years, in terms of PCE and stability,[9−13] but DSSCs based on ruthenium(II)-polypyridine complexes still have record-high PCE values (>11%).[2] Among various organic/inorganic sensitizers, Ru-$(H_2dcbpy)_2(NCS)_2$ and $[Ru(Htctpy)(NCS)_3](TBA)_3$ hold the credit as benchmark sensitizers; these are widely known as N3 and black dye, respectively. Recently, a certified record efficiency of 11.4% has been reported using a simple coadsorbent in a black-dye-based test cell.[14] To further improve the photovoltaic parameters, our group and other research groups have developed a series of tripyridine ruthenium dyes. Most of the ruthenium photosensitizers contain the thiocyanate

Received: July 27, 2013
Accepted: November 4, 2013
Published: November 4, 2013

(SCN) ligand, which make sensitizers unstable, which triggered investigations to replace thiocyanate with other effective chelating chromophores in the ruthenium dyes.[15−18] Although, initially, the DSSCs based on the thiocyanate-free ruthenium-based dyes showed limited successes,[19−22] PCE values of 10.1% and 9.54% has been achieved with a new sensitizer by incorporating 2,4-difluorophenyl pyridinato ancillary ligands[23] and pyridyl pyrazolate ancillaries.[24] In search of new sensitizers, van Koten,[19,25] Berlinguette,[26] and the Gratzel group[27−29] have independently investigated varieties of ruthenium(II)-based polypyridine complexes with tridentate cyclometalating chelate as sensitizers for DSSCs.[30] As a part of our research program, in the development of thiocyanate-free ruthenium complex dyes,[15,31−33] we have reported a PCE of 7.96%, using a thiocyanate-free ruthenium(II) dye as a sensitizer for the DSSCs.[34]

Herein, we report the synthesis and characterization of a new thiocyanate-free ruthenium complex, **SPS-G3**, which contains 2,6-bis (1-methylbenzimidazol-2-yl)pyridine and has been used as a sensitizer for DSSCs. We have achieved an overall PCE of 6.04% with TiO_2 photoanode and enhanced up to 7.72% with the same electrolyte and counter electrode, when MWCNT/TiO_2 nanocomposite film was used as a photoanode.

EXPERIMENTAL SECTION

Synthesis of Thiocyanate-Free Sensitizers SPS-G3. In a typical experiment, [Ru(triethoxycarbonylterpy)Cl_3] (290 mg, 0.4419 mmol), 2,6-bis(1-methylbenzimidazol-2-yl)pyridine (150 mg, 0.4419 mmol), and 4-ethyl morpholine (0.141 mL, 1.104 mmol) were dissolved in EtOH (30 mL).[35,36] The mixture was refluxed for 4 h under constant stirring. After the removal of solvent, the residue was extracted with CH_2Cl_2 (3 mL), washed with water and concentrated to dryness. The crude product was further purified by silica gel column chromatography (hexane/ethyl acetate = 1:1). After then, the resulting solid was dissolved in a mixture of acetone (50 mL) and 1.5 M NaOH solution (6.2 mL). The reaction mixture was heated to 60 °C for 6 h under N_2 atmosphere. The solvent was removed, and the resulting residue was dissolved in H_2O solution (10 mL). This solution was titrated with 2 N HCl to pH value of 3 to afford a black precipitate. The precipitate filtered to obtain solid as pure complex.

^1H NMR. ($CDCl_3$ + CD_3OD, 300 MHz, δ) 9.48−9.46 (m, 2H), 9.03−9.01 (m, 6H), 7.86−7.80 (m, 6H), 7.62−7.58 (m, 3H), 7.51−7.50 (m, 1H), 7.39−7.36 (m, 3H), 7.07−7.03 (m, 2H), 3.36 (s, 6H); IR (KBr, cm^{-1}) 3398, 3085, 2923, 2852, 1708, 1603, 1475, 1418, 1355, 1234, 1161, 1019, 746.

Fabrication of Dye-Sensitized Solar Cells. A double-layer TiO_2 photoelectrode with a 14-μm-thick transparent nanoporous layer of TiO_2 particles ~20 nm in size and a 4-μm-thick scattering layer (area: 0.25 cm^2) was prepared by screen printing on the precleaned fluorine-doped indium oxide (FTO) glass substrate and then sintered at 450 °C for 30 min as reported earlier.[37−40] MWCNTs (purity >95%, diameter = 20 nm) were purchased from Sigma−Aldrich. The MWCNT−TiO_2 composite films were prepared as follows, and the MWCNTs were functionalized with COOH groups, as described in the literature.[56]

Commercially available titanium(IV) tetra-isopropoxide (TTIP) (>98%) was obtained from Aldrich. The MWCNT−TiO_2 composite paste was prepared as follows. The TiO_2 paste was first prepared by using a mixture of TTIP and P25 TiO_2 at a molar ratio of 0.08/1 in ethanol. The acid-treated MWCNTs in different quantities were subjected to ultrasonication, along with the TiO_2 paste, for 30 min and stirred for 2 h. The composite paste was coated on an FTO substrate using the doctor blade technique and then dried at room temperature, followed by sintering at 450 °C for 20 min.

A scattering layer (4 μm) was then applied over the MWCNT−TiO_2 composite layer. The electrodes were impregnated with a 0.1 M aqueous solution of titanium tetrachloride solution to block the FTO glass electrode from coming into direct contact with the electrolyte, thus preventing the recombination, and were again sintered at 450 °C for 20 min. For the dye sensitization, the prepared photoanodes were dipped into the dye solution (3×10^{-4} M concentration in acetonitrile/*tert*-butyl alcohol (1/1) with deoxycholic acid (DCA) (20 mM)) for 12 h. The TiO_2 film, which was coated with a sensitizer, was separated by a Surlyn spacer (40 μm thick) from a platinum-coated conducting glass. The polymer frame was sealed by heating. The device fabrication was completed by inserting the electrolyte consisting of a solution of 0.6 M dimethylpropyl-imidazolium iodide (DMPII), 0.05 M I_2, 0.1 M LiI, and 0.5 M *tert*-butylpyridine (TBP) in acetonitrile.

The current−voltage (J−V) of DSSCs was measured illuminating the device through a xenon source (AM 1.5G simulated, 100 mW cm^{-2}) and the computer-controlled Keithley source meter. The effective area of the devices was 0.25 cm^2. The incipent photon-to-current efficiency (IPCE) for the DSSC was recorded on a Model CEP-2000 system (Bunkoh-Keiki Co., Ltd.).

A potentiostat/galvanostat (PGSTAT 30, Autolab, Eco-Chemie) was employed to measure the electrochemical impedance spectra (EIS) of the DSSCs in darkness as well as under illumination (100 mW cm^{-2}) in the frequency range from 10 mHz to 100 kHz. The DC and AC biases applied to the DSSC are near the equivalent to the open-circuit voltage of the DSSC and 10 mV, respectively. The impedance spectra were analyzed by an equivalent circuit, using Z-view software.

RESULTS AND DISCUSSION

Chemical structure of **SPS-G3** is shown in Scheme 1. The synthesis of the new sensitizer in one-pot reaction was carried out as mentioned in the Experimental Section. UV−visible absorption spectra of **SPS-G3** in DMF solution and on TiO_2 film are shown in Figure 1. Among two absorption bands observed, below 350 nm is attributed to intraligand π−π^* transitions of [2,2′:6′,2″-terpyridine]-4,4′,4″-tricarboxylic acid and ancillary ligand, and an absorption band having a peak at ~498 nm is attributed to metal-to-ligand charge transfer (MLCT) transition. When **SPS-G3** is anchored onto the surface of the TiO_2 film, the absorption peak corresponding to MLCT is significantly red-shifted (absorption peak at 517 nm) and broadened, which clearly reveals that the dyed TiO_2 film is able to absorb the visible light from 350 to 700 nm effectively. The optical band gap of the **SPS-G3** estimated from the onset of its absorption spectra adsorbed onto TiO_2 film is ~1.86 eV, which is slightly lower than that estimated from the cyclic voltammetry.

It is well-known that the 2,6-bis(1-methylbenzimidazol-2′-yl)pyridine acts as a hybrid ligand, having both strong σ-donor (benzimidazole unit) and π-acceptor (pyridine ring) properties. Thus, by appropriate choice of the substituents on the

Scheme 1. Chemical Structure of SPS-G3.

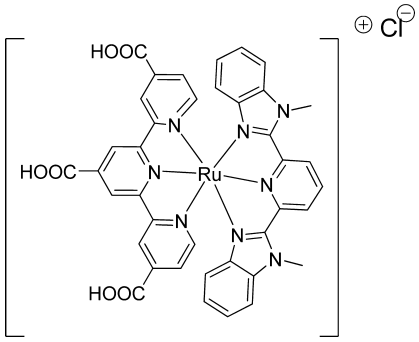

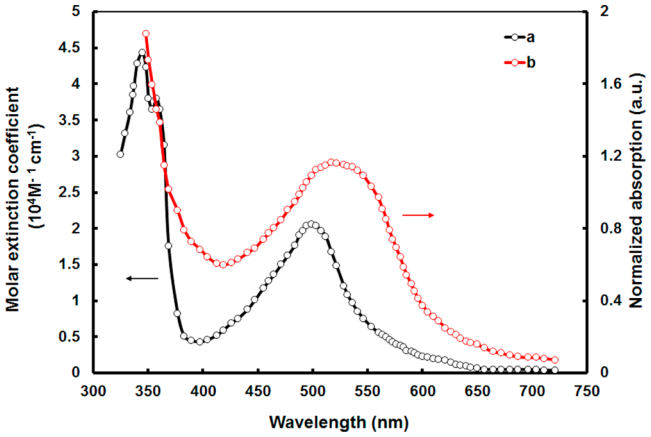

Figure 1. Absorption spectra of (a) **SPS-G3** dye in DMF solution and (b) **SPS-G3** adsorbed onto TiO_2 film.

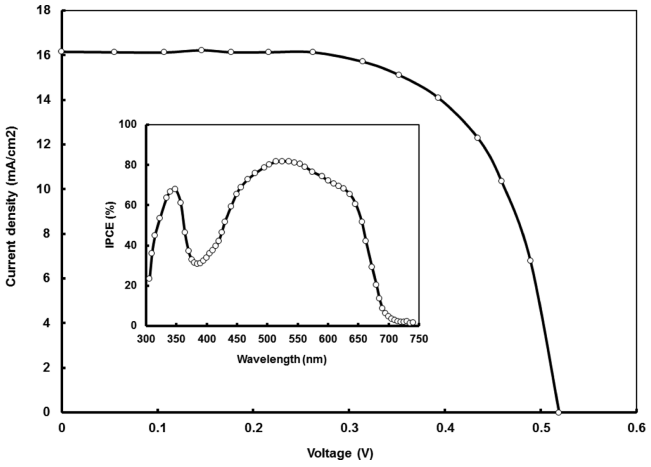

Figure 2. Current−voltage (J−V) curve under AM 1.5G simulated solar light at a light intensity of 100 mW cm^{-2} with a metal mask of 0.25 cm^2 with TiO_2 photoanode. The insert the IPCE spectra of the DSSC sensitized with **SPS-G3** is also shown.

Table 1. Photovoltaic Parameters of the DSSCs Sensitized with SPS-G3 Dye Employing Pristine TiO_2 and MWCNT (0.3 wt %)−TiO_2 Photoanodes

photoanode	short-circuit density, J_{sc} (mA/cm^2)	open circuit voltage, V_{oc} (V)	fill factor, FF	power conversion efficiency, PCE (%)
		SPS-G3		
TiO_2	16.15	0.52	0.72	6.05
MWCNTs (0.3 wt %)−TiO_2	18.24	0.56	0.76	7.76
		N719		
TiO_2	14.74	0.61	0.72	6.47
MWCNTs (0.3 wt %)−TiO_2	16.38	0.63	0.76	7.84

imidazole nitrogen, it is possible to tune the LUMO and HOMO levels in a more predictable manner. The carboxyl groups of the terpyridine ligand provide the grafting onto the oxide surface ensuring an intimate electron coupling between the sensitizer and semiconductor. This type of electron interaction is required to facilitate the rapid electron transfer from the excited state of sensitizer to the TiO_2 conduction band.

We have estimated the HOMO and LUMO energy levels from the cyclic voltammetry. The reduction potential corresponds to the LUMO energy level (−1.03 V vs NHE) of **SPS-G3** is more negative than the conduction band of TiO_2 (−0.5 V vs NHE)[41−43] indicates driving force is sufficient for the electron injection from the LUMO level of **SPS-G3** into the conduction band of TiO_2. The ground-state potential corresponds to the HOMO level of **SPS-G3** and is ∼0.87 eV vs NHE, which is more positive than the redox potential of the I^-/I_3^- couple (0.5 V vs NHE)[44−47] in electrolyte for efficient dye regeneration. The electrochemical band gap estimated from the difference in HOMO and LUMO energy levels, is ∼1.90 eV.

The photocurrent density−voltage (J−V) curve and the IPCE plot of the DSSC sensitized with **SPS-G3** are shown in Figure 2 and the photovoltaic parameters are summarized in Table 1. In this table, we have also included the photovoltaic parameters for the DSSC sensitized with N719 dye, for comparison. The DSSC sensitized with **SPS-G3** showed J_{sc} = 16.15 mA/cm^2, V_{oc} = 0.52 V, and fill factor (FF = 0.72), resulting in an overall PCE of 6.04%. The maximum IPCE of the DSSC was ∼82% at a wavelength of 524 nm. This wavelength corresponds to the maximum absorption peak of the **SPS-G3** adsorbed on the TiO_2 surface. The PCE is low, compared to the other Ru(II)-based dyes, which is attributed to the low absorption in the wavelength range 350−425 nm and competitive absorption of photons in this region by the redox couple.

Generally, in DSSCs, the photogenerated electrons injected from the excited state of the dye into the conduction band of mesoporous TiO_2 electrode, encounter many grain boundaries while passing through the TiO_2 nanoparticle network and, hence, enhances the probability of recombination which is responsible for the decreasing the photocurrent and PCE. Therefore, it is necessary to prevent these recombination processes to increase the PCE of DSSCs. One promising solution to prevent back recombination processes at TiO_2/dye/electrolyte interface is to use the one-dimensional (1D) nanostructure photoanode by replacing the nanoparticle film, which provides a direct pathway for the collection of electrons injected in the conduction band of TiO_2 in the device.[48−50] Another approach involves the incorporation of highly conductive materials such as carbon nanotubes and graphite in the TiO_2 photoanode. The presence of these conductive materials in the TiO_2 network is expected to improve the charge transport properties, thereby improving the PCE of the DSSCs. Many research groups have reported that incorporation of these conductive materials in the TiO_2 matrix enhances the electron transport and the collection efficiency.[51,52] MWCNTs have excellent mechanical properties, electrical conductivity, and thermal conductivity, and these properties make them a potential advanced nanocomposite material with improved functions, including large surface area, stable structure, and good conductivity.[53] The unique characteristics of MWCNTs, such as their electron-accepting capability[54] and electron storage capability, also makes them ideal for sequestering photogenerated electrons.[50,55−63] It is believed that performance of the DSSCs can be improved when MWCNTs are incorporated into the photoanode oxide. Recent reports demonstrated that the use of MWCNTs in the TiO_2-based photoanode has improved the performance of DSSCs.[64]

We have characterized the MWCNT−TiO_2 composite by employing the Raman spectra. Figure 3 shows the Raman

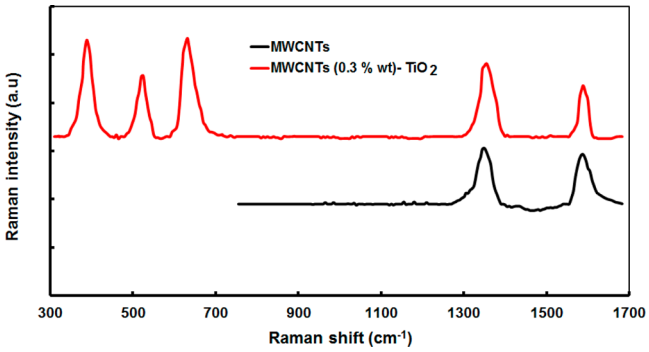

Figure 3. Comparison of Raman spectra of MWCNTs and MWCNT (0.3 wt %)−TiO_2 nanocomposite.

spectra of MWCNT and MWCNT−TiO_2 composite. In contrast with the Raman spectra of MWCNTs, the MWCNT−TiO_2 nanocomposite shows five peaks with the Raman peak of 388 cm^{-1}, 526 cm^{-1} and 632 cm^{-1} associated with TiO_2[59,65,66] and other two peaks at 1354 cm^{-1} (D-band) and 1588 cm^{-1} (G band) of the MWCNT peak.[67] As shown in the figure, the D-band and G-band peaks corresponding to the MWCNT of MWCNT/TiO_2 composite show blue shifts, by 8 cm^{-1} and 4 cm^{-1}, respectively, relative to that of pristine MWCNT at ∼1346 cm^{-1} and 1584 cm^{-1}. These blue shifts can be attributed to the strain effects of the TiO_2/MWCNTs interfaces, which may influence the vibrational frequencies.[68] Moreover, these Raman spectral changes of MWCNTs, are due to the adherence of TiO_2 nanoparticles to the MWCNTs.

We have incorporated MWCNTs into the TiO_2 matrix and used it as photoanode for the DSSC using the **SPS-G3** dye. The concentration of MWCNTs has been varied in TiO_2 matrix and found that the optimized concentration is 0.3 wt %. Beyond this concentration, the PCE of the device starts to decrease, which implies that the incorporation of small amount of the MWCNTs into the TiO_2 is sufficient to enhance the photovoltaic response. We have also measured the dye loading using the absorption spectra of desorbed dye from the photoanodes and found that beyond this concentration (0.3%) of MWCNTs the dye loading reduces (the optimum dye loading for pristine TiO_2 and 0.3 wt % MWCNTs TiO_2 is 2.05×10^{-7} mol cm^{-2} and 2.56×10^{-7} mol cm^{-2}, respectively, after that dye loading starts decreasing), resulting in lesser electrons injected from dye into the MWCNT−TiO_2 composite electrode.[4,69,70]

Therefore, we have investigated the detailed characterization of DSSC based on MWCNT−TiO_2 photoanode only. The current−voltage characteristics and IPCE spectra of the DSSC based on MWCNT (0.3 wt %)−TiO_2 composite films are shown in Figure 4 and the photovoltaic parameters are compiled in Table 1. It was found that the photovoltaic performance strongly affected by the incorporation of MWCNTs in the TiO_2 matrix. Compared to the DSSC with TiO_2 photoanode, the device with the incorporation of MWCNTs (0.3 wt %) into TiO_2 paste exhibits higher photovoltaic parameters i.e., J_{sc}, V_{oc} and FF, leading to over all PCE of 7.76%. The value of V_{oc} increases from 0.52 V to 0.56 V with an increase of MWCNT from 0 to 0.3 wt %. The photovoltaic parameters for the DSSC sensitized with N719

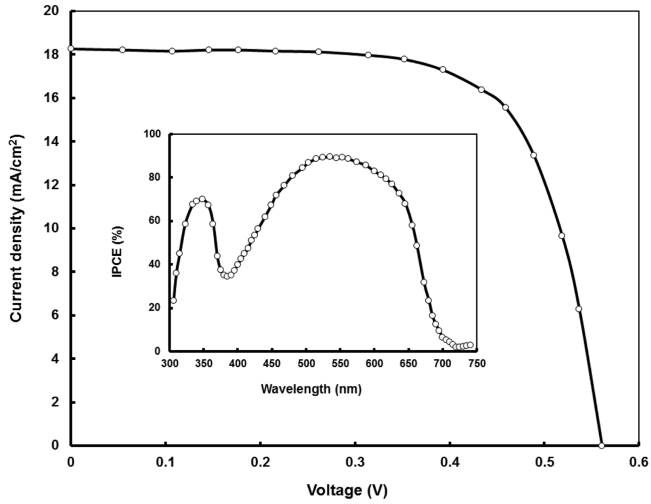

Figure 4. Current−voltage (J−V) curve under AM 1.5G simulated solar light at a light intensity of 100 mW cm^{-2} with a metal mask of 0.25 cm^2 for DSSC with MWCNT−TiO_2 photoanode and in the insert the IPCE spectra of the DSSC sensitized with **SPS-G3** is also shown.

dye and MWCNT−TiO_2 photoanode are also included in Table 1. Similar tends of increase in PCE have been observed for this device also. The addition of a small amount of MWCNTs into the TiO_2 can reduce the charge recombination rate and charge transport resistance, as discussed in the EIS data. The existence of MWCNTs in TiO_2 increased the FF of DSSC from 0.72 to 0.76, which is attributed to the increase in the conductivity of TiO_2 photoanode. This result was supported by the EIS analysis described later. The IPCE values at each wavelength are also higher for the DSSC based on MWCNT−TiO_2 photoanode, which is consistent with J_{sc}, since J_{sc} is directly proportional to IPCE. The IPCE can be expressed as

$$\mathrm{IPCE}(\lambda) = \mathrm{LHE}(\lambda)\eta_{inj}\eta_{cc}$$

where $\mathrm{LHE}(\lambda)$ is the light harvesting efficiency of the dye-sensitized photoanode at wavelength (λ) and is dependent on the absorption profile of the dye and dye loading by the photoanode, η_{inj} is the efficiency for the electron injection from the LUMO level of sensitizer into the conduction band of TiO_2, and η_{cc} is the electron collection efficiency. Dye adsorption capability is dependent on the surface area of the photoanode. We have recorded the absorption spectra of the **SPS-G3** adsorbed onto both pristine TiO_2 film and MWCNT−TiO_2 film and found that the molar extinction coefficient is almost the same, which indicates that there is no noticeable difference in the amount of dye adsorbed molecules in the pristine TiO_2 vs MWCNT−TiO_2 photoanode. The amount of dye adsorbed at the surface of the pristine TiO_2 photoanode and MWCNT−TiO_2 photoanode is estimated to be 4.57×10^{-6} mol/cm^2 and 4.62×10^{-6} mol/cm^2, respectively. Since the dye loading for the MWCNT−TiO_2 photoanode is slightly higher than that for pristine TiO_2, the increased value of J_{sc} and IPCE in the MWCNT−TiO_2-based DSSC therefore is not only a result from an increased amount of dye adsorbed onto the MWCNT−TiO_2: there are other factors also responsible for the increase in these parameters. Another possible reason for the enhancement in the J_{sc} and PCE may be other factors, i.e., η_{inj} and η_{cc}. η_{inj} is related to the energy difference between the

LUMO energy level of the sensitizer and the conduction band edge of metal oxide, i.e., TiO_2 (ΔE_{inj}) used in photoanode.[71] The larger value of ΔE_{inj} can generate the stronger driving force to facilitate the electron injection from the LUMO of the sensitizer into the conduction band of TiO_2.[49] Since the conduction band edge of the MWCNT (~0 eV vs NHE) is much lower than that of TiO_2 (−0.5 V vs NHE), but the potential of MWCNTs is higher than that of TiO_2, the charge equilibrium between two materials in the MWCNT−TiO_2 composite would cause a shift of apparent Fermi level to a more-positive potential (i.e., downward shift).[72,73] Therefore, after the charge equilibrium, the conduction band edge of the MWCNT−TiO_2 composite will also shift to more-positive values, compared to that of pristine TiO_2. This will increase the value of ΔE_{inj} and leads to enhancement of the charge injection efficiency. In the MWCNT/TiO_2 composite film, electron injected into the TiO_2 may easily migrate to the MWCNTs, because of the withdrawing nature of MWCNTs[56,74,75] The charge collection efficiency may also be increased for MWCNTs/TiO_2 photoanode with the help of the highly conductive 1D carbon nanotubes.

The V_{oc} of a DSSC is theoretically the difference between the Fermi level (E_F) of the oxide semiconductor employed in the photoanode under illumination and the Nernst potential of I^-/I_3^- redox couple. As mentioned above, E_F shifted downward after the inclusion of MWCNTs and which caused a loss in V_{oc}. However, the V_{oc} has been improved for the DSSCs with a MWCNT/TiO_2 photoanode. Therefore, the improved electron injection and suppressed charge recombination compensate for the loss in photovoltage, leading to an increase in V_{oc}.

The electrochemical impedance spectra (EIS) has been employed to explain the exact cause for the improvement in J_{sc} and PCE for MWCNTs/TiO_2-based DSSC, compared to that observed for pristine TiO_2-based DSSC. The EIS values of DSSCs under illumination (100 mW/cm^2) at a voltage equivalent to the V_{oc} based on pristine TiO_2 and MWCNT−TiO_2 photoanode are shown in Figure 5. The Nyquist plots (Figure 5a) of the EIS spectra exhibit three semicircles, which represents to the electrochemical reaction at the Pt/electrolyte interface in the high-frequency region, to the charge transfer at the TiO_2/dye interface in the middle-frequency region, and to the Warburg diffusion process of I^-/I_3^- in the electrolyte in the low-frequency region.[76] The overall series resistance (R_s) is the resistance measured when electrons are transported through the device in the high-frequency range exceeding 10^5 Hz. The Nyquist plots (Figure 5a) showed that the R_s value decreased from 18.5 Ω to 11.6 Ω as MWCNTs were incorporated into the TiO_2, which increased the conductivity of the TiO_2 film, resulting in a decrease in the R_s of the DSSC. The semicircle in the middle-frequency region is assigned to charge transport at TiO_2/dye/electrolyte interface. Compared with that of TiO_2-based DSSC, the value of the charge-transport resistance (R_{tran}) at the TiO_2/dye/electrolyte interface of MWCNT−TiO_2-based DSSC significantly decreases from 31 Ω to 22 Ω. It is due to the fact that the 1D MWCNTs favor the photoinjected electron transfer faster, thus lowering the charge recombination.[77−79]

As shown in Bode phase plots of EIS (Figure 5b), the characteristics peaks in the frequency region (1−10^2 Hz) showed that the characteristic frequency peak shifted to a lower frequency for MWCNT/TiO_2-based DSSCs, compared to pristine TiO_2-based DSSC. The characteristic frequency peak is related to the inverse of the recombination lifetime or electron lifetime in the TiO_2 film.[80,81] The electron lifetime estimated

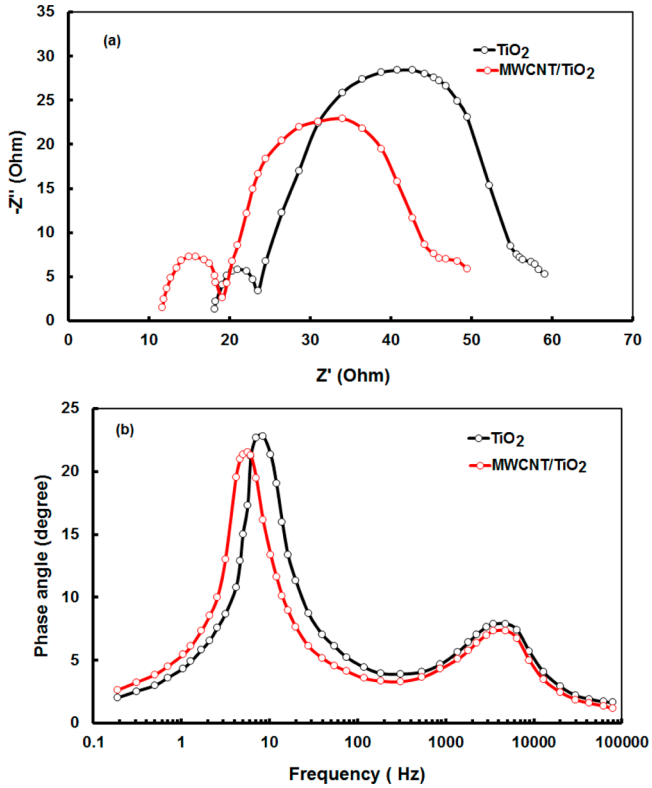

Figure 5. Electrochemical impedance spectroscopy (EIS) spectra: (a) Nyquist plots and (b) Bode phase plots for DSSCs sensitized with **SPS-G3** employing pristine TiO_2 and MWCNT (0.3 wt %)−TiO_2 photoanodes, under illumination (100 mW/cm^2) at a bias voltage equivalent to the open-circuit voltage (V_{oc}).

from the characteristic frequency peak was 18.8 and 26.5 ms for TiO_2 and MWCNT/TiO_2-based DSSCs, respectively. This implies that the collection and transport of electrons were faster with the incorporation of MWCNTs into TiO_2 matrix, thereby reducing the electron recombination and extending the electron lifetime in TiO_2 film.

The Nyquist plots of the DSSCs based on TiO_2 and MWCNT−TiO_2 photoanodes measured in darkness at an applied voltage equivalent to the V_{oc} are shown in Figure 6. The values of the charge recombination resistance (R_{rec}) estimated

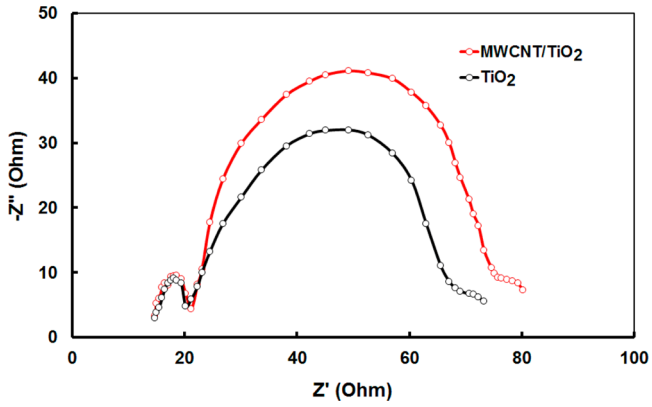

Figure 6. Nyquist plots of EIS of DSSCs sensitized with **SPS-G3**, employing pristine TiO_2 and MWCNT (0.3 wt %)−TiO_2 photoanodes in darkness at a voltage equivalent to the open circuit voltage (V_{oc}).

from the real impedance component of the intermediate frequency semicircle were ~42 Ω and 53 Ω for the TiO_2/dye/electrolyte interface and the MWCNT−TiO_2/dye/electrolyte interface, respectively. The high charge recombination resistance at the MWCNT−TiO_2/dye/electrolyte interface in darkness means that the charge recombination between injected electrons and the electron acceptors in the electrolyte is low. From the Nyquist plots of the DSSCs in darkness and under illumination, it is found that a decrease in R_{tran} and an increase in R_{rec} was observed after the incorporation of MWCNTs in the MWCNT−TiO_2 composite. A smaller value of R_{rec}, in theory, means faster recombination between electrons in TiO_2 and electron acceptors in electrolyte and, thus, a shorter electron lifetime.[82]

In order to understand the increase in J_{sc} and V_{oc} for the MWCNT−TiO_2 photoanode, compared to the pristine TiO_2 photoanode, we have also measured the J−V characteristics of the both DSSCs in darkness; this experiment is shown in Figure 7. It can be seen from Figure 7 that the value of the darkness

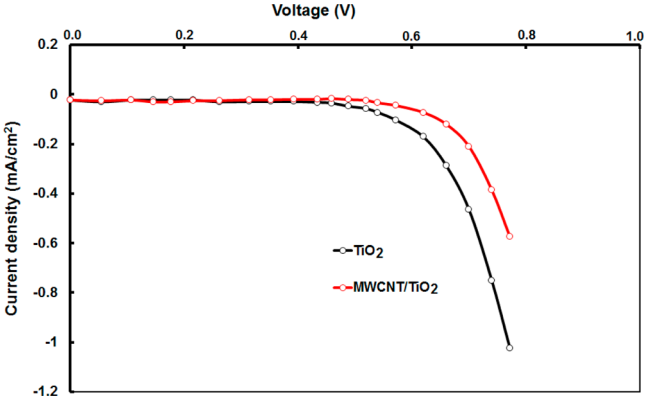

Figure 7. Current−voltage (J−V) characteristics of the DSSCs with different photoanodes, in darkness.

current for the DSSC with a MWCNT−TiO_2 photoanode is smaller than that for pristine TiO_2. Moreover, the onset potential also shifts toward higher potential for the MWCNT−TiO_2 photoanode, compared to the pristine TiO_2 photoanode. This indicates that, with the incorporation of MWCNTs into TiO_2, the conduction band edge shifts in the downward direction (more positive), relative to pristine TiO_2. The darkness current in the DSSCs is a measure of recombination between injected electrons and I_3^- in the electrolyte at the photoanode/dye/electrolyte interface. A smaller darkness current is critical for high values of both V_{oc} and J_{sc} in DSSCs.[83] When the MWCNT−TiO_2-based DSSC is compared to the pristine TiO_2, the former exhibits a smaller darkness current, which indicates that recombination of the photoinjected electrons with I_3^- has been suppressed significantly, which favors the increase in V_{oc}. The enhancement in V_{oc} is generally associated with the negative shift (upward) of the conduction band of TiO_2 or suppression of electron recombination with I_3^-. As the conduction band edge of the MWCNT−TiO_2 shifts upward, compared to TiO_2, the loss in V_{oc} is compensated by the suppression of electron recombination, resulting in an enhancement in V_{oc}. The suppression of in the back electron recombination also results in the charge collection efficiency; thereby, the value of J_{sc} has been increased.

We have also estimated the electron transport time (τ_d) from the EIS data in darkness and under illumination, using the following expression:

$$\frac{\tau_d}{\tau_n} = \frac{R_{tran}}{R_{rec}}$$

The electron transport time is a measure of the average time taken for the collection of injected electrons; a faster electron transport time is associated with a higher photocurrent, since it indicates that the electrons hop across the TiO_2 network and are collected at the photoanode at a faster rate.[84] The decrease in R_{tran} and increase in R_{rec} as the MWCNTs was incorporated into the TiO_2, which indicates that the electron transport time has been decreased for the DSSC based on the MWCNT−TiO_2 photoanode. This means the electrons are reaching the FTO substrate faster in this improved device, compared to TiO_2-based DSSCs, as the electron transport rate is enhanced. The effective diffusion coefficient (D_{eff}) of an electron in the photoanode of a DSSC can be estimated from the following expression:[85]

$$D_{eff} = \left(\frac{R_{rec}}{R_{tran}}\right)\left(\frac{L^2}{\tau_n}\right)$$

where L is the thickness of the TiO_2 film. The value of D_{eff} for DSSC, based on MWCNT−TiO_2 (14 nm) was larger than that for pristine TiO_2 (10.65 nm). The higher D_{eff} value for the MWCNT−TiO_2-based DSSC could be explained by more injected electrons and faster induced transport of the electrons toward the FTO substrate.

The improvement in the PCE is due to the decrease in charge transport resistance at the TiO_2/dye/electrolyte interface; the decreased charge recombination of photoinjected electrons and efficient charge transport of electrons by MWCNTs enhances the transport of electrons from the TiO_2 film to the FTO substrate.

CONCLUSION

In summary, we prepared a new ruthenium-based thiocyanate-free photosensitizer containing 2,6-bis(1-methylbenzimidazol-2-yl)pyridine and coded as **SPS-G3** and successfully used it for dye-sensitized solar cells (DSSCs) with an overall power conversion efficiency (PCE) of 6.04% under simulated air mass (AM) 1.5 sunlight. We have incorporated multiwalled carbon nanotubes (MWCNTs) into the TiO_2 and used it as a photoanode to improve the photovoltaic performance of DSSC. Different concentrations of MWCNTs in TiO_2 on the device performance have been investigated, and the optimum concentration was determined to be 0.3 wt %. The PCE has been increased up to 7.76% when a MWCNT−TiO_2 photoanode is used instead of TiO_2. The increase in PCE is due to the improved electron charge transport and reduction in the charge recombination with MWCNTs as efficient electron acceptors in electrolyte.

AUTHOR INFORMATION

Corresponding Author

*E-mail: spsingh@iict.res.in.

Notes

The authors declare no competing financial interest.

■ ACKNOWLEDGMENTS

S.P.S. thanks the DST for support through the Fast Track Young Scientist Project (No. CS-83/2012).

■ REFERENCES

(1) Listorti, A.; O'Regan, B.; Durrant, J. R. *Chem. Mater.* **2011**, *23*, 3381−3399.
(2) O'Regan, B.; Grätzel, M. *Nature* **1991**, *353*, 737−740.
(3) Hagfeldt, A.; Grätzel, M. *Acc. Chem. Res.* **2000**, *33*, 269−277.
(4) Grätzel, M. *Acc. Chem. Res.* **2009**, *42*, 1788−1798.
(5) Yum, J. H.; Walter, P.; Huber, S.; Rentsch, D.; Geiger, T.; Nüesch, F.; Angelis, F. D.; Grätzel, M.; Nazeeruddin, M. K. *J. Am. Chem. Soc.* **2007**, *129*, 10320−10321.
(6) Ito, S.; Zakeeruddin, S. M.; Robin, H.-B.; Liska, P.; Charvet, R.; Comte, P.; Nazeeruddin, M. K.; Péchy, P.; Takata, M.; Miura, H.; Uchida, S.; Grätzel, M. *Adv. Mater.* **2006**, *18*, 1202−1205.
(7) Hagfeldt, A.; Grätzel, M. *Chem. Rev.* **1995**, *95*, 49−68.
(8) Gao, F.; Wang, Y.; Zhang, J.; Shi, D.; Wang, M.; Robin, H.-B.; Wang, P.; M. Zakeeruddin, S.; Grätzel, M. *Chem. Commun.* **2008**, 2635−2637.
(9) Hagfeldt, A.; Boschloo, G.; Sun, L. C.; Kloo, L.; Pettersson, H. *Chem. Rev.* **2010**, *110*, 6595−6663.
(10) Mishra, A.; Fischer, M. K.; Bauerle, P. *Angew. Chem., Int. Ed.* **2009**, *48*, 2474−2499.
(11) Zeng, W.; Cao, Y.; Bai, Y.; Wang, Y.; Shi, Y.; Zhang, M.; Wang, F.; Pan, C.; Wang, P. *Chem. Mater.* **2010**, *22*, 1915−1925.
(12) Ooyama, Y.; Harima, Y. *Chem. Phys. Chem* . **2012**, *13*, 4032−4080.
(13) Yen, Y. S.; Chou, H. H.; Chen, Y. C.; Hsu, C. Y.; Lin, J. T. *J. Mater. Chem.* **2012**, *22*, 8734−8747.
(14) Han, L.; Islam, A.; Chen, H.; Malapaka, C.; Chiranjeevi, B.; Zhang, S.; Yang, X.; Yanagida, M. *Energy Environ. Sci.* **2012**, *5*, 6057−6060.
(15) Singh, S. P.; Islam, A.; Yanagida, M.; Han, L. *Int. J. Photoenergy* **2011**, Article 520848 (5 pp).
(16) Numata, Y.; Singh, S. P.; Islam, A.; Iwamura, M.; Imai, A.; Nozaki, K.; Han, L. *Adv. Funct. Mater.* **2013**, *23*, 1817−1823.
(17) Nguyen, P. T.; Degn, R.; Nguyen, H. T.; Lund, T. *Sol. Energy Mater. Sol. Cells* **2009**, *93*, 1939−1945.
(18) Asghar, M. I.; Miettunen, K.; Halme, J.; Vahermaa, P.; Toivola, M.; Aitola, K.; Lund, P. *Energy Environ. Sci.* **2010**, *3*, 418−426.
(19) Wadman, S. H.; Kroon, J. M.; Bakker, K.; Lutz, M.; Spek, A. L.; Van Klink, G. P. M.; Van Koten, G. *Chem. Commun.* **2007**, 1907−1909.
(20) Wadman, S. H.; Lutz, M.; Tooke, D. M.; Spek, A. L.; Hartl, F.; Havenith, R. W. A.; Van Klink, G. P. M.; Van Koten, G. *Inorg. Chem.* **2009**, *48*, 1887−1900.
(21) Bomben, P. G.; Robson, K. C. D.; Sedach, P. A.; Berlinguette, C. P. *Inorg. Chem.* **2009**, *48*, 9631−9643.
(22) Koivisto, B. D.; Robson, K. C. D.; Berlinguette, C. P. *Inorg. Chem.* **2009**, *48*, 9644−9652.
(23) Bessho, T.; Yoneda, E.; Yum, J.-H.; Guglielmi, M.; Tavernelli, I.; Imai, H.; Rothlisberger, U.; Nazeeruddin, M. K.; Grätzel, M. *J. Am. Chem. Soc.* **2009**, *131*, 5930−5934.
(24) Wu, K. L.; Hsu, H.-C.; Hen, C. K.; Yun, C.; Chung, M.-W.; Liub, W.-H.; Chou, P.-T. *Chem. Commun.* **2010**, *46*, 5124−5126.
(25) Wadman, S. H.; Kroon, J. M.; Bakker, K.; Hevenith, R. W. A.; Van Klink, G. P. M.; Van Koten, G. *Organometallics* **2010**, *29*, 1569−1579.
(26) Bomben, P. G.; Theriault, K. D.; Berlinguette, C. P. *Eur. J. Inorg. Chem.* **2011**, 1806−1814.
(27) Robson, K. C. D.; Koivisto, B. D.; Yella, A.; Sporinova, B.; Nazeeruddin, M. K.; Baumgartner, T.; Grätzel, M.; Berlinguette, C. P. *Inorg. Chem.* **2011**, *50*, 5494−5508.
(28) Wu, K. L.; Ku, W. P.; Wang, S. W.; Yella, A.; Chi, Y.; Liu, S. H.; Chou, P. T.; Nazeeruddin, M. K.; Grätzel, M. *Adv. Funct. Mater.* **2013**, *23*, 2285−2294.
(29) Wu, K.-L.; Ku, W.-P.; Clifford, J. N.; Palomares, E.; Ho, S.-T.; Yun, Chi.; Liu, S.-H.; Chou, P.-T.; Nazeeruddin, M. K.; Grätzel, M. *Energy Environ. Sci.* **2013**, *6*, 859−870.
(30) Wu, K. L.; Li, C. H.; Chi, Y.; Clifford, J. N.; Cabau, L.; Palomares, E.; Cheng, Y. M.; Chou, P. T. *J. Am. Chem. Soc.* **2012**, *134*, 7488−7496.
(31) Islam, A.; Singh, S. P.; Han, L. *Funct. Mater. Lett.* **2011**, *4*, 21−24.
(32) Chou, C. C.; Wu, K.-L.; Chi, Y.; Hu, W.-P.; Yu, S. J.; Lee, G.-H.; Lin, C.-L.; Chou, P.-T. *Angew. Chem., Int. Ed.* **2011**, *50*, 2054−2058.
(33) Wang, S.-W.; Wu, K.-L.; Ghadiri, E.; Lobello, M. G.; Ho, S.-T.; Chi, Y.; Moser, J.-E.; Angelis, F. D.; Grätzel, M.; Nazeeruddin, M. K. *Chem. Sci.* **2013**, *4*, 2423−2433.
(34) Singh, S. P.; Gupta, K. S. V.; Sharma, G. D.; Islam, A.; Han, L. *Dalton Trans.* **2012**, *41*, 7604−7608.
(35) Nazeeruddin, M. K.; Péchy, P.; Renouard, T.; Zakeeruddin, S. M.; Robin, H.-B.; Comte, P.; Liska, P.; Cevey, L.; Costa, E.; Shklover, V.; Spiccia, L.; Deacon, G. B.; Bignozzi, C. A.; Grätzel, M. *J. Am. Chem. Soc.* **2001**, *123*, 1613−1624.
(36) Mathew, I.; Sun, W. *Dalton Trans.* **2010**, *39*, 5885−5898.
(37) Johansson, P.; Rowley, J.; Taheri, A.; Meyer, G. J.; Singh, S. P.; Islam, A.; Han, L. *Langmuir* **2011**, *27*, 14522−14531.
(38) Gao, S.; Islam, A.; Numata, Y.; Han, L. *Appl. Phys. Express* **2010**, *3*, 062301−062303.
(39) Islam, A.; Singh, S. P.; Han, L. *Int. J. Photoenergy* **2011**, Article No. 204639 (8 pp).
(40) Akhtaruzzaman, M.; Islam, A.; Fan, Y.; Asao, N.; Kwon, E.; Singh, S. P.; Han, L.; Yamamoto, Y. *Chem. Commun.* **2011**, *47*, 12400−12402.
(41) Klein, C.; Nazeeruddin, M. K.; Censo, D. D.; Liska, P.; Grätzel, M. *Inorg. Chem.* **2004**, *43*, 4216−4226.
(42) Chang, Y. J.; Chow, T. J. *Tetrahedron* **2009**, *65*, 9626−9632.
(43) Zhang, G. L.; Bai, Y.; Li, R. Z.; Shi, D.; Wenger, S.; Zakeeruddin, S. M.; Grätzel, M.; Wang, P. *Energy Environ. Sci.* **2009**, *2*, 92−95.
(44) Kang, S. H.; Choi, S. H.; Kang, M. S.; Kim, J. Y.; Kim, H. S.; Hyen, T.; Sung, Y. E. *Adv. Mater.* **2008**, *20*, 54−58.
(45) Yang, L.; Leung, W. W .F. *Adv. Mater.* **2011**, *23*, 4559−4562.
(46) Varghese, O. K.; Paulose, M.; Grimes, C. A. *Nat. Nanotechnol.* **2009**, *4*, 592−597.
(47) Krishnamorthy, T.; Thavasi, V.; Subodh, M.; Ramakrishna, G. S. *Energy Environ. Sci.* **2011**, *4*, 2807−2812.
(48) Yang, N.; Zhai, J.; Wang, D.; Chen, Y.; Jiang, L. *ACS Nano* **2010**, *4*, 3778−3787.
(49) Kongkanand, A.; Dominguez, R. M.; Kamat, P. V. *Nano Lett.* **2007**, *7*, 676−680.
(50) Dang, X.; Yi, H.; Ham, M. H.; Qi, J.; Yun, D. S.; Ladewski, R.; Strano, M. S.; Hammond, P. T.; Belcher, A. M. *Nat. Nanotechnol.* **2011**, *6*, 377−384.
(51) Flahaut, E.; Peigney, A.; Laurent, C.; Marliere, C.; Chastel, F.; Rousset, A. *Acta Mater.* **2000**, *48*, 3803−3812.
(52) Peng, C.; Snook, G. A.; Fray, D. J.; Shaffer, M. S.; Chen, G. Z. *Chem. Commun.* **2006**, *44*, 4629−4631.
(53) Woan, K.; Pyrgiotakis, G.; Sigmund, W. *Adv. Mater.* **2009**, *21*, 2233−2239.
(54) Kongkanand, A.; Kamat, P. V. *ACS Nano* **2007**, *1*, 13−21.
(55) Yen, C. Y.; Lin, Y. F.; Liao, S. H.; Weng, C. C.; Husang, C. C.; Hsiao, Y. H.; Ma, C. C.; Chang, M. C.; Shao, H.; Tsai, M. C.; Hsieh, C. K.; Tsai, C. H.; Weng, F. B. *Nanotechnology* **2008**, *19*, 375305.
(56) Lee, K. M.; Hu, C. W.; Chen, H. W.; Ho, K. C. *Sol. Energy Mater. Sol. Cells* **2008**, *92*, 1628−1633.
(57) Muduli, S.; Lee, W.; Dhas, V.; Mujawar, S.; Dubey, M.; Vijaysmohanan, K.; Han, S. H.; Ogale, S. *ACS Appl. Mater. Interfaces* **2009**, *1*, 2030−2035.
(58) Lin, W. J.; Hsu, C. T.; Tsai, Y. C. *J. Colloid Interface Sci.* **2011**, *358*, 562−566.
(59) Yu, J. G.; Fan, J. J.; Cheng, B. *J. Power Sources* **2011**, *196*, 7891−7898.
(60) Zhu, P. N.; Nair, A. S.; Yang, S. Y.; Peng, S. J.; Elumalai, N. K.; Ramakrishna, S. *J. Photochem. Photobiol., A* **2012**, *231*, 9−18.

(61) Nath, N. C.; Sarker, S.; Ahemmad, A. J. S.; Lee, J. J. *Phys. Chem. Chem. Phys.* **2012**, *14*, 4333−4338.
(62) Chen, J. Z.; Li, B.; Cheng, J. F.; Zhao, J. H.; Zhu, Z. P. *J. Phys. Chem. C* **2012**, *116*, 14848−14856.
(63) Chen, T.; Qiu, L. B.; Cai, Z. B.; Gong, F.; Yang, Z. B.; Wang, Z. S.; Peng, H. S. *Nano Lett.* **2012**, *12*, 2568−2572.
(64) Hu, G. J.; Meng, X. F.; Feng, X. Y.; Ding, Y. F.; Zhang, S. M.; Yang, M. S. *J. Mater. Sci.* **2007**, *42*, 7162−7170.
(65) Sawatsuk, T.; Chindaduang, A.; Sae-kung, C.; Pratontep, S.; Tumcharern, G. *Diamond Relat. Mater.* **2009**, *18*, 524−527.
(66) Rai, P.; Mohapatra, R.; Hazra, K. S.; Mishra, D. S.; Ghatak, J.; Satyam, P. V. *Chem. Phys. Lett.* **2008**, *455*, 83−87.
(67) Xu, C. Y.; Zhang, P. X.; Yan, L. *J. Raman Spectrosc.* **2001**, *32*, 862−865.
(68) Ivan, M.-S.; Gimenez, S.; Francisco, F.-S.; Gomez, R.; Shen, Q.; Toyoda, J.; Bisquert, T. *Acc. Chem. Res.* **2009**, *42*, 1848−1857.
(69) Grätzel, M. *Inorg. Chem.* **2005**, *44*, 6841−6851.
(70) Kang, S. H.; Kim, J. Y.; Kim, Y. Y.; Kim, H. S.; Sung, Y. E. *J. Phys. Chem. C* **2007**, *111*, 9614−9623.
(71) Frank, A. J.; Kopidakis, N.; van de Lagemaat, J. *Coord. Chem. Rev.* **2004**, *248*, 1165−1179.
(72) Xiang, Q. J.; Yu, J. G.; Jaroniec, M. *Nanoscale* **2011**, *3*, 3670−3678.
(73) Xiang, Q. J.; Yu, J. G.; Jaroniec, M. *Chem. Soc. Rev.* **2012**, *41*, 782−796.
(74) Wang, Q.; Moser, J. E.; Grätzel, M. *J. Phys. Chem. B* **2005**, *109*, 14945−14953.
(75) Yanagida, S.; Yu, Y. H.; Manseki, K. *Acc. Chem. Res.* **2009**, *42*, 1827−1838.
(76) Yu, J. G.; Ma, T. T.; Liu, S. W. *Phys. Chem. Chem. Phys.* **2011**, *13*, 3491−3501.
(77) Schlichthorl, G.; Huang, S. Y.; Sprague, J.; Frank, A. J. *J. Phys. Chem. B* **1997**, *101*, 8141−8155.
(78) Schlichthorl, G.; Park, N. G.; Frank, A. J. *J. Phys. Chem. B* **1999**, *103*, 782−791.
(79) Kern, R.; Sastrawan, R.; Ferber, J.; Stangl, R.; Luther, J. *Electrochim. Acta* **2002**, *47*, 4213−4225.
(80) Francisco, F.-S.; Bisquert, J.; Germa, G.-B.; Boschloo, G.; Hagfeldt, A. *Sol. Energy Mater. Sol. Cells* **2005**, *87*, 117−131.
(81) Goes, M. S.; Joanni, E.; Muniz, E. C.; Savu, R.; Habeck, T. R.; Bueno, P. R.; Francisco, F.-S. *J. Phys. Chem. C* **2012**, *116*, 12415−12421.
(82) Ito, S.; Liska, P.; Comte, P.; Charvet, R.; Péchy, P.; Bach, U.; Schmidt-Mende, L.; Zakeeruddin, S. M.; Kay, A.; Nazeeruddin, M. K.; Grätzel, M. *Chem. Commun.* **2005**, 4351−4353.
(83) Wang, Q.; Zhang, Z.; Zakeeruddin, S. M.; Grätzel, M. *J. Phys. Chem. C* **2008**, *112*, 7084−7092.
(84) Langemaat, J. V.; Frank, A. J. *J. Phys. Chem. B* **2000**, *104*, 4292−4294.
(85) Adachi, M.; Sakamoto, M.; Jiu, J. T.; Ogata, Y.; Isoda, S. *J. Phys. Chem. B* **2006**, *110*, 13872−13880.